

Article

Simple Fabrication of Hydrophobicity-Controlled Fe-ZSM-5 for Aqueous-Phase Partial Oxidation of Methane with Hydrogen Peroxide

Seok Young Hwang ¹, Minjae Kwon ¹, Jongkook Hwang ^{1,2,*} and Eun Duck Park ^{1,2,*}

¹ Department of Energy Systems Research, Ajou University, Suwon 16499, Republic of Korea; sog9690@ajou.ac.kr (S.Y.H.); minjae4816@ajou.ac.kr (M.K.)

² Department of Chemical Engineering, Ajou University, Suwon 16499, Republic of Korea

* Correspondence: jongkook@ajou.ac.kr (J.H.); edpark@ajou.ac.kr (E.D.P.); Tel.: +82-31-219-2384 (E.D.P.); Fax: +82-31-219-1612 (E.D.P.)

Abstract: Surface hydrophobicity is an important factor in controlling the catalytic activity of heterogeneous catalysts in various reactions, particularly liquid-phase reactions using water as the (co)solvent. In this study, the surface hydrophobicity of Fe-ZSM-5 was successfully controlled using a simple coating method in which furfuryl alcohol was used as the carbon precursor. Various techniques, such as N₂ physisorption, temperature-programmed desorption of ammonia, and contact angle measurements of water droplets, were used to characterize the catalysts. Fe-ZSM-5 catalysts with different degrees of hydrophobicity were used for the aqueous-phase selective oxidation of methane with H₂O₂. The positive effect of the surface carbon coating on the catalytic performance was confirmed when the carbon content was not sufficiently high to block the pores.

Keywords: hydrophobicity; Fe-ZSM-5; methane; aqueous-phase oxidation; hydrogen peroxide



Citation: Hwang, S.Y.; Kwon, M.; Hwang, J.; Park, E.D. Simple Fabrication of Hydrophobicity-Controlled Fe-ZSM-5 for Aqueous-Phase Partial Oxidation of Methane with Hydrogen Peroxide. *Catalysts* **2024**, *14*, 280. <https://doi.org/10.3390/catal14040280>

Academic Editors: Zhijun Zuo, Lei Liu and Ines Graca

Received: 25 February 2024

Revised: 13 April 2024

Accepted: 18 April 2024

Published: 20 April 2024



Copyright: © 2024 by the authors. Licensee MDPI, Basel, Switzerland. This article is an open access article distributed under the terms and conditions of the Creative Commons Attribution (CC BY) license (<https://creativecommons.org/licenses/by/4.0/>).

1. Introduction

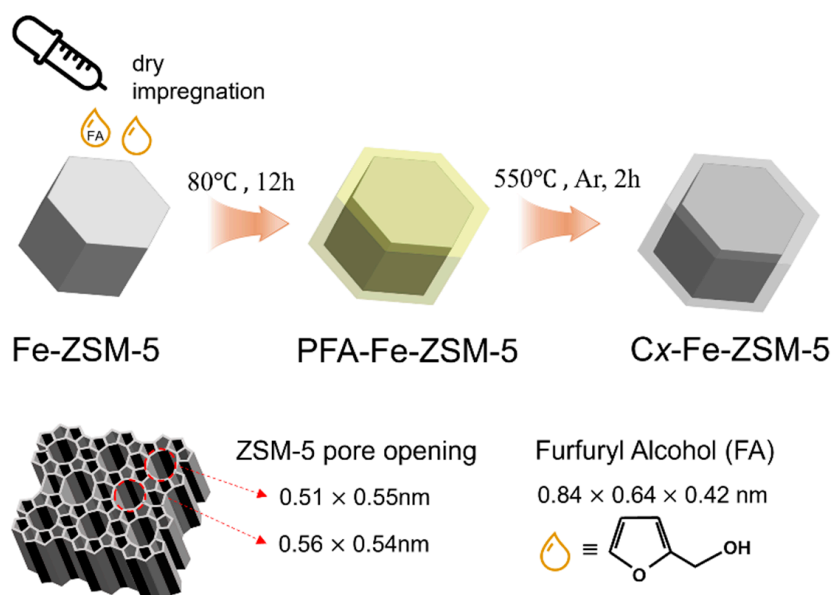
Surface hydrophobicity is an important factor that affects the performance of heterogeneous catalysts for various reactions. In particular, low-temperature gas-phase reactions, in which water is used as a reactant or product, [1,2] and liquid-phase reactions, in which water serves as a (co)solvent [3,4], are strongly influenced by the surface hydrophobicity of the catalyst. Therefore, various techniques, such as surface coating, surface grafting, surface etching, and space structure modification, have been adopted to control the surface hydrophobicity of catalysts [5].

The aqueous-phase selective oxidation of hydrocarbons has attracted considerable attention as an environmentally friendly route to produce value-added products. In particular, the selective oxidation of methane in water with hydrogen peroxide has been intensively studied over the last decade because methane is a relatively clean and abundant resource [6–8]. Inspired by enzymes (e.g., soluble and particulate methane monooxygenases) that can oxidize methane into methanol with dioxygen in the presence of reducing agents under ambient conditions [9], various biomimetic heterogeneous catalysts, such as Fe- and Cu-zeolites, have been examined for the aqueous-phase oxidation of methane with H₂O₂ [10–27] or in situ-generated H₂O₂ from H₂ and O₂ [28–33]. In addition to biomimetic heterogeneous catalysts, AuPd-based catalysts have recently been developed for this reaction [34–40]. These catalysts not only generate H₂O₂ from H₂ and O₂ but can also activate the C–H bonds of methane with H₂O₂ generated in situ to produce methane oxygenates, including methanol.

Although the liquid-phase selective oxidation of methane with H₂O₂ has been performed in water, to the best of our knowledge, only the Xiao group has applied a catalyst with controlled surface hydrophobicity for this reaction [41]. They reported high catalytic

activity for this reaction with in situ-generated H₂O₂ from H₂ and O₂ over AuPd alloy nanoparticles encapsulated within zeolites modified with organosilanes [41]. The main reason for this productivity improvement is that the hydrophobic silane confined H₂O₂ inside the catalyst, maintaining a high local concentration of H₂O₂. However, the effect of hydrophobicity on the aqueous-phase partial oxidation of methane by H₂O₂ is not completely understood. Furthermore, the complexity of the silane modification process and reliance on precious metals provide opportunities for developing better catalysts that are potentially more cost-effective and simpler.

In this study, we report a simple carbon-coating method for controlling the surface hydrophobicity of zeolites. To minimize the effects of other factors on the catalyst properties, Fe-ZSM-5 was used as the parent catalyst to further control surface hydrophobicity. Surface hydrophobicity was controlled by the amount of furfuryl alcohol (FA) used. FA was chosen because its molecular size ($0.84 \text{ nm} \times 0.64 \text{ nm} \times 0.42 \text{ nm}$) is larger than the micropore size ($0.54 \text{ nm} \times 0.56 \text{ nm}$) of the ZSM-5 so that it can be mainly deposited onto the external surface of ZSM-5 (Scheme 1). Furthermore, FA is in the liquid state, allowing for direct dry impregnation without the need for additional solvents. FA is polymerized through acid-catalyzed condensation at the external acid sites of ZSM-5 and is then converted to carbon upon pyrolysis in an N₂ atmosphere. The prepared catalysts were characterized by N₂ physisorption, temperature-programmed desorption of ammonia (NH₃-TPD), and water droplet contact angle measurements. The aqueous-phase oxidation of methane with H₂O₂ was performed over these catalysts, and their catalytic activities were compared. The promotional effect of the surface carbon coating on the catalytic performance was evident when the carbon content was sufficiently moderate not to block the pores and Fe-active sites.



Scheme 1. Illustration of the surface modification of Fe-ZSM-5.

2. Results and Discussion

2.1. Characterization of Catalysts

The Fe contents of H-ZSM-5 and Fe-ZSM-5 were 0.014 and 0.52 wt.%, respectively. The presence of Fe in the H-ZSM-5 zeolite is a natural phenomenon arising from the inadvertent inclusion of trace amounts of Fe during zeolite preparation. This is consistent with the findings of previous studies [11]. To investigate the different Fe species present in the catalysts, the UV–Vis spectra of H-ZSM-5 and Fe-ZSM-5 were collected and analyzed (Figure S1). The UV–Vis spectrum of H-ZSM-5 displayed nearly one band within the 250–350 nm range. In contrast, the spectrum of Fe-ZSM-5 exhibited a broad band that extended up to 600 nm. The absorption bands of Fe-ZSM-5 generally fall into three

categories: (i) 250–350 nm, indicative of either isolated or oligonuclear extra-framework Fe species; (ii) 350–450 nm, characteristic of iron oxide clusters; and (iii) above 450 nm, associated with larger iron oxide aggregates located on the external surface of the crystal. The fraction of each Fe species was estimated and is presented in Table S1. This analysis revealed that the Fe species in H-ZSM-5 consisted predominantly of isolated or oligonuclear extra-framework Fe species (Figure S1a) [42,43]. Similarly, the primary Fe species in Fe-ZSM-5 were isolated or oligonuclear extra-framework Fe species, even though iron oxide clusters and aggregates were present in Fe-ZSM-5, in agreement with the conventional Fe-ZSM-5 catalyst [20,21]. These specific Fe species (isolated or oligonuclear extra-framework Fe species) are the main active sites for the partial oxidation of methane with H_2O_2 in the aqueous phase [30].

The carbon contents of carbon-coated H-ZSM-5 and Fe-ZSM-5 were measured by elemental analysis and are reported in Table 1. The carbon contents of Cx-H-ZSM-5 and Cx-Fe-ZSM-5 were 0.22–2.70 wt.% and 0.27–4.84 wt.%, respectively. SEM-EDX revealed the homogeneous deposition of carbon species on the external surfaces of the catalysts (Figure S2).

Table 1. The textural properties of all catalysts.

Catalyst ^a	BET Surface Area (m^2/g)	Micropore Surface Area (m^2/g)	Pore Volume (cm^3/g)	Micropore Volume (cm^3/g)
H-ZSM-5	355	280	0.20	0.127
C0.22-H-ZSM-5	315	210	0.22	0.095
C0.30-H-ZSM-5	310	199	0.23	0.092
C0.45-H-ZSM-5	308	204	0.23	0.094
C1.27-H-ZSM-5	277	204	0.20	0.093
C1.78-H-ZSM-5	281	211	0.20	0.097
C2.31-H-ZSM-5	244	183	0.18	0.083
C2.70-H-ZSM-5	186	142	0.16	0.065
Fe-ZSM-5	267	187	0.18	0.085
C0.27-Fe-ZSM-5	250	201	0.17	0.092
C0.62-Fe-ZSM-5	252	186	0.18	0.085
C1.08-Fe-ZSM-5	254	194	0.17	0.089
C1.50-Fe-ZSM-5	251	195	0.18	0.089
C2.30-Fe-ZSM-5	253	189	0.18	0.087
C3.41-Fe-ZSM-5	222	177	0.16	0.081
C4.84-Fe-ZSM-5	188	150	0.14	0.069

^a The carbon content in each catalyst was measured by elemental analysis.

The textural properties of the prepared catalysts were analyzed from N_2 physisorption data and are listed in Table 1. In the Cx-H-ZSM-5 series, as the carbon content increased, there was a trend of decreasing BET specific surface area (SSA_{BET}), micropore surface area, pore volumes, and micropore volumes. The changes in SSA_{BET} according to carbon content (x) are shown in Figure S3. In the Cx-H-ZSM-5 series, the decrease in SSA_{BET} was relatively small at low carbon contents (0.22~0.45 wt.%) (Figure S3a). However, when the carbon content exceeded 1 wt.%, the SSA_{BET} decreased considerably. A similar, yet slightly different trend was observed for Cx-Fe-ZSM-5. Compared to Cx-H-ZSM-5, Cx-Fe-ZSM-5 generally exhibited a lower SSA_{BET} and micropore volume owing to the incorporation of Fe species within the H-ZSM-5 framework. In Cx-Fe-ZSM-5, SSA_{BET} remained relatively constant across a wide range of carbon contents, from 0.27 to 2.3 wt.%. This is presumed to be due to the preoccupation of micropores by Fe species, which impedes the blocking of these micropores by post-carbon deposition. A notable decrease in SSA_{BET} was observed when the carbon content exceeded 3 wt.% in Cx-Fe-ZSM-5. These results suggest that the blocking of micropores due to carbon deposition predominantly occurred when the carbon content exceeded 1.27 wt.% in Cx-H-ZSM-5 and 3.41 wt.% in Cx-Fe-ZSM-5. There was no noticeable change in the pore size distribution of mesopores with different carbon contents

(Figure S4), suggesting that the blockage of micropores is the main cause of the decrease in surface area and pore volume of carbon-coated catalysts.

The effect of the carbon coating on the surface acidity of the catalysts was investigated using NH₃-TPD. The surface acid sites of aluminosilicates catalyze the polycondensation of FA [44]. Thus, the polycondensation of FA primarily occurred at the acidic sites of ZSM-5, implying that carbon deposition could cover the acidic sites and subsequently reduce their concentration. The NH₃-TPD spectra of the parent H-ZSM-5 and Cx-H-ZSM-5 samples with different carbon contents are shown in Figure 1. The NH₃-TPD spectra of the parent H-ZSM-5 and Cx-H-ZSM-5 catalysts were deconvoluted into two peaks, and the results are listed in Figure S5 [45,46]. The low-temperature peak with a maximum at 201 °C corresponded to the weak acid sites. In contrast, the high-temperature peak corresponding to the strong acid sites had the maximum at 349 °C. As the carbon content in Cx-H-ZSM-5 increased, the peak areas of both the low- and high-temperature peaks decreased. As the peak area is directly related to the amount of desorbed NH₃, (i.e., total number of acid sites), the quantitative amount of adsorbed NH₃ for each catalyst was calculated and is presented in Table S2. The total number of acid sites decreased slightly with increasing carbon content in Cx-H-ZSM-5; however, the difference between the catalysts was almost negligible for samples with carbon contents ranging from 0.30 to 2.31 wt%. A similar trend was observed in the NH₃-TPD spectrum of Cx-Fe-ZSM-5 (Figure 2) [47–50]. The number of weak, strong, and total acid sites tended to decrease only slightly with an increase in carbon content (Figure S6 and Table S3). The overall surface acidity is rather comparable to each other among the Cx-Fe-ZSM-5 catalysts.

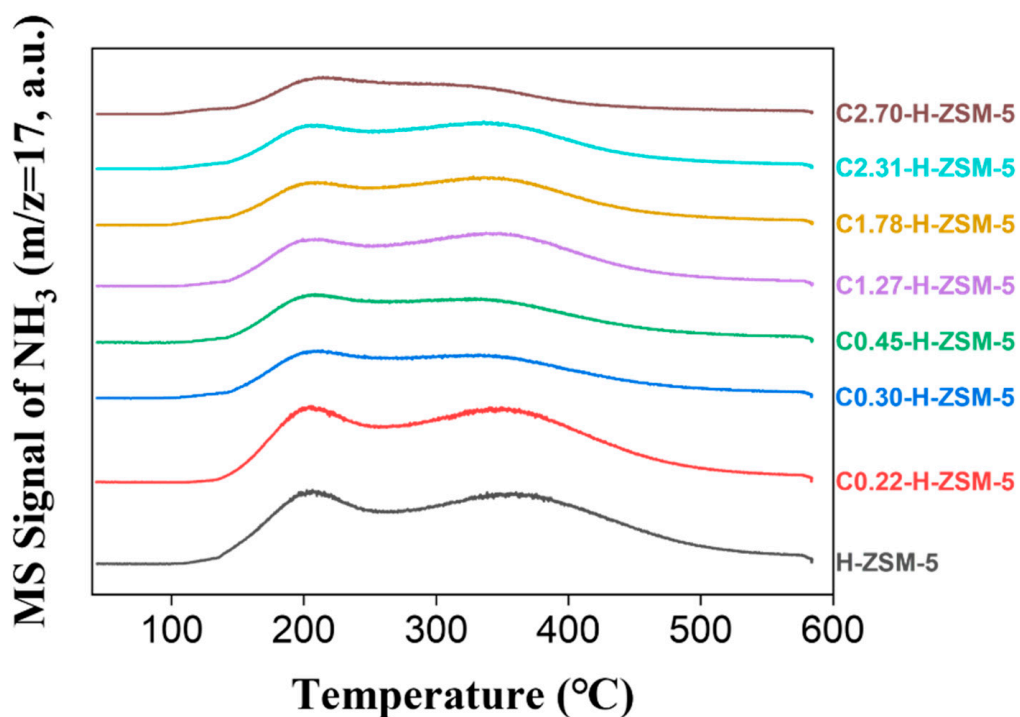


Figure 1. NH₃-TPD profiles for H-ZSM-5 and carbon-coated H-ZSM-5 with different carbon contents.

The influence of the carbon coating on the surface hydrophobicity (i.e., water wettability) of the catalysts was investigated by measuring the contact angles of water droplets for H-ZSM-5, Cx-H-ZSM-5, Fe-ZSM-5, and Cx-Fe-ZSM-5. As shown in Figure 3, the contact angle of H-ZSM-5 was 11.6°, which increased with increasing carbon content in Cx-H-ZSM-5. Similarly, the contact angle for Fe-ZSM-5 was 17.2°, which increased with the carbon content in Cx-Fe-ZSM-5. The average value of the contact angle for each sample is listed in Table S4. This indicates that the surface hydrophobicity of both Cx-H-ZSM-5 and Cx-Fe-ZSM-5 increased almost linearly with carbon content [51–54]. Since the difference

in the contact angles of water droplets for the samples with low carbon contents is not noticeable, temperature-programmed desorption of water ($\text{H}_2\text{O-TPD}$) profiles for H-ZSM-5 and carbon-coated H-ZSM-5 with low carbon contents were additionally obtained. As the carbon content increased, the peak temperature shifted to the lower temperature and the peak intensity decreased (Figure S7). These data also show that the surface hydrophobicity of the catalyst increases with carbon content [1]. The Fourier-transform infrared (FT-IR) spectra of H-ZSM-5 and carbon-coated H-ZSM-5 reveal the presence of $-\text{C}-\text{H}$ (CH_2) species on the carbon-coated H-ZSM-5 (Figure S8).

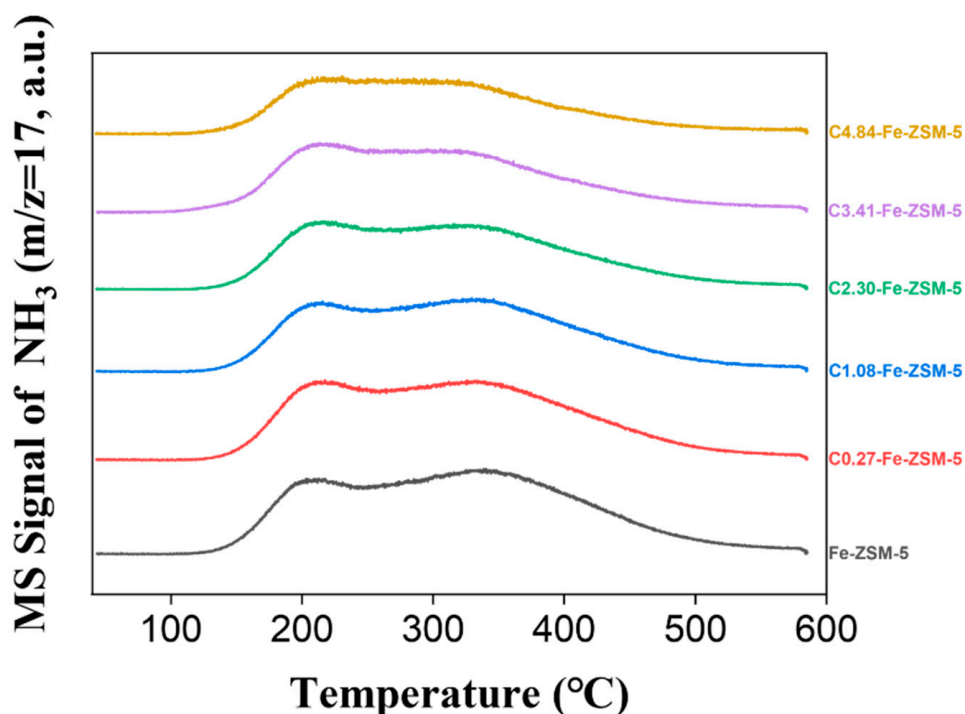


Figure 2. NH_3 -TPD profiles for Fe-ZSM-5 and carbon-coated Fe-ZSM-5 with different carbon contents.

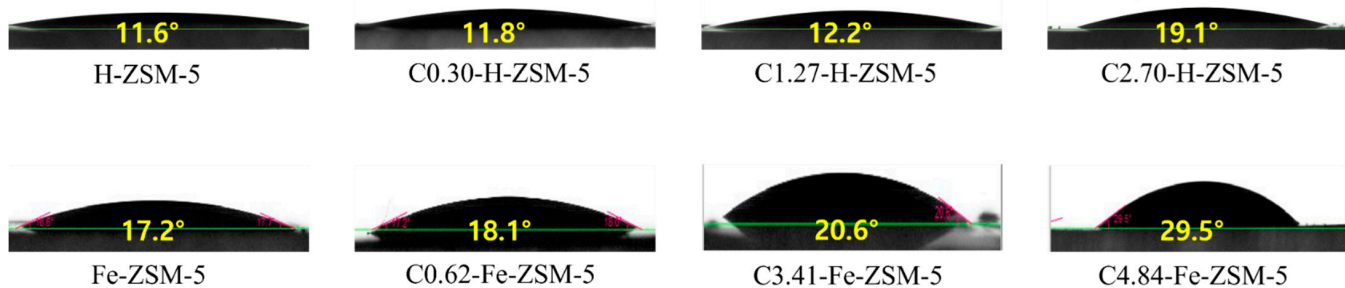


Figure 3. The contact angle of the water droplet for H-ZSM-5, Fe-ZSM-5, carbon-coated H-ZSM-5, and carbon-coated Fe-ZSM-5.

2.2. Catalytic Performance of Catalysts

The aqueous-phase oxidation of methane with H_2O_2 was performed over the H-ZSM-5 and Cx-H-ZSM-5 with different carbon contents. As shown in Figure 4, the catalytic performance depends on the carbon content of Cx-H-ZSM-5 . The promoting effect of carbon coating on the synthesis of methane oxygenate was observed in the Cx-H-ZSM-5 series. With increasing carbon content, the total product yield initially rose, peaking at $x = 0.45$, and then began to decrease (Figure 4a). For instance, C0.45-H-ZSM-5 exhibited an approximately 50% increase in the total product yield compared to H-ZSM-5. Furthermore, the total product yield per amount of consumed H_2O_2 was evaluated (Figure 4b) as it is directly related to H_2O_2 utilization efficiency. A similar volcano-type relationship was

observed between carbon content and total product yield per unit of consumed H_2O_2 (Figure 4b). Despite the significant differences in product yield, the product selectivity was comparable among the catalysts, indicating that carbon deposition had a minor influence on product selectivity (Figure S9). In all cases, HCOOH was the predominant product of methane oxygenation. In terms of both the total product yield and H_2O_2 utilization efficiency, C0.45-H-ZSM-5 was the most effective catalyst in the Cx-H-ZSM-5 series.

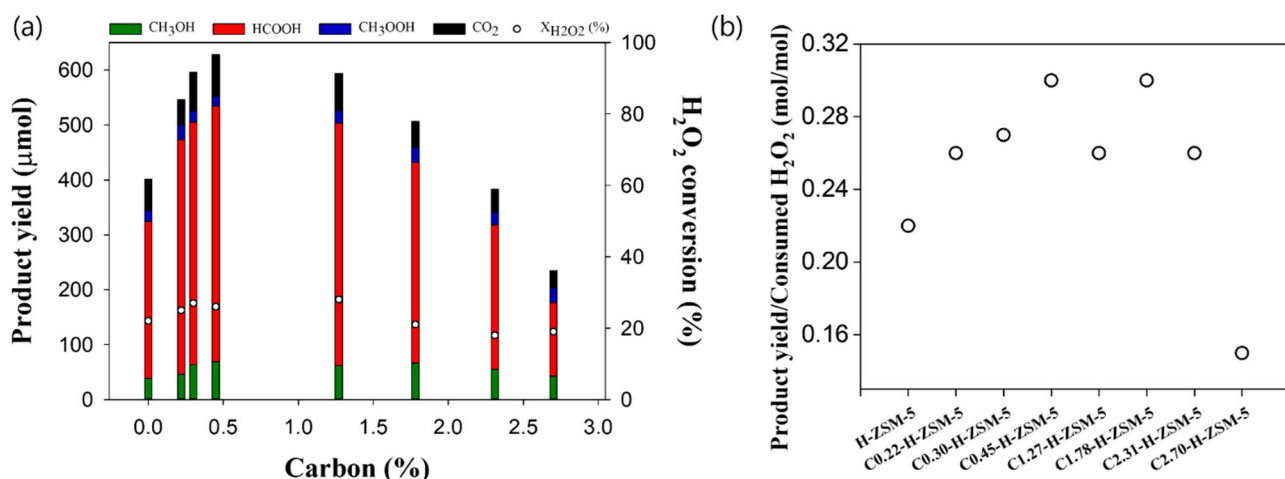


Figure 4. The catalytic performance for the aqueous-phase partial oxidation of methane over H-ZSM-5 and Cx-H-ZSM-5 with different carbon contents. **(a)** Total product yield and H_2O_2 conversion ($X_{\text{H}_2\text{O}_2}(\%)$) and **(b)** total product yield normalized per H_2O_2 consumed. Reaction conditions: 30 mL of H_2O , 95 mL of CH_4 at 31 bar, 0.277 M H_2O_2 , 100 mg of catalyst, reaction temperature = 50 °C, and reaction time = 1 h.

The impact of the carbon coating on Cx-Fe-ZSM-5 was also assessed because Fe-ZSM-5 is a typical catalyst used for the aqueous-phase partial oxidation of methane [10,14,15,22,23]. Since Fe-ZSM-5 has a higher amount of active Fe species than H-ZSM-5 due to the difference in Fe content (Figure S1 and Table S1), the catalytic activity of Fe-ZSM-5 and carbon-coated Fe-ZSM-5 was measured at a lower temperature than that of H-ZSM-5. A noticeable promoting effect of the carbon coating was also observed for Cx-Fe-ZSM-5, as shown in Figure 5. Even minimal carbon deposition (0.27 wt.%) results in a significant increase in the total product yield and H_2O_2 conversion (Figure 5a). C0.62-Fe-ZSM-5 exhibited the highest product yield and H_2O_2 utilization efficiency in Cx-Fe-ZSM-5 (Figure 5b). When the carbon content exceeded 0.62 wt.%, the overall catalytic performance began to slowly degrade. However, Cx-Fe-ZSM-5 maintained a similarly high catalytic performance over a broad range of carbon contents from 0.27 to 2.3 wt.%. The product selectivity was similar for Fe-ZSM-5 and Cx-Fe-ZSM-5 ($x = 0.27\text{--}2.3$), and in all cases, HCOOH was the main methane oxygenate product (Figure S10). This result is consistent with that of Cx-H-ZSM-5, further indicating that carbon deposition has a negligible effect on product selectivity. Notably, even C4.84-Fe-ZSM-5, which showed the lowest catalytic performance in the Cx-Fe-ZSM-5 series, exhibited superior product yield and H_2O_2 utilization efficiency compared to Fe-ZSM-5, strongly indicating the promoting effect of the carbon coating on the synthesis of methane oxygenates.

Furthermore, in the recycling tests conducted for the representative Fe-ZSM-5 and C1.08-Fe-ZSM-5 catalysts, both demonstrated stable catalytic performances across all three rounds of testing, as shown in Figure 6.

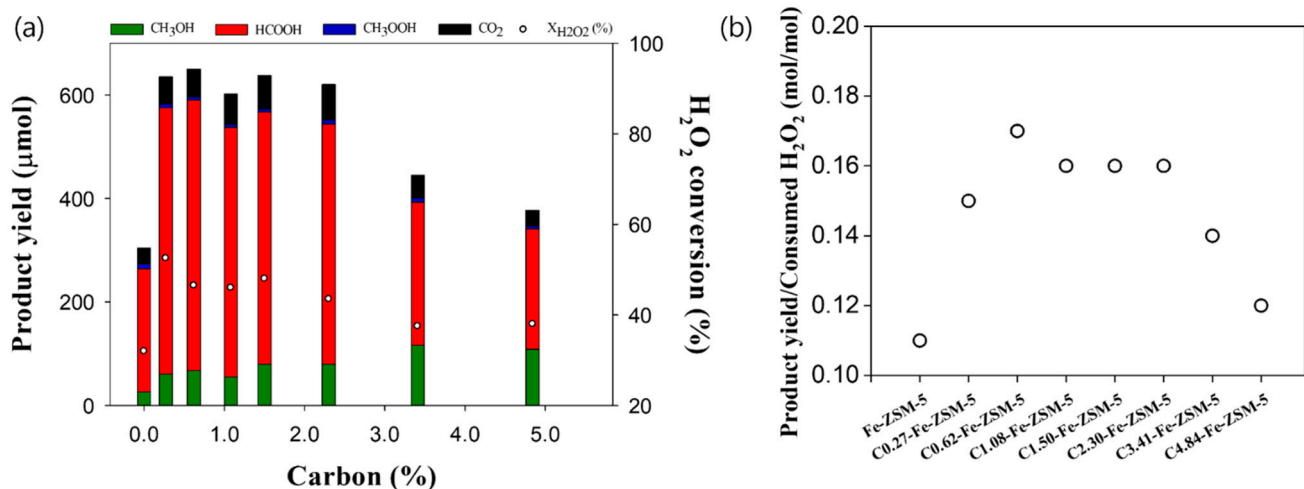


Figure 5. The catalytic performance for the aqueous-phase partial oxidation of methane over Fe-ZSM-5 and Cx-Fe-ZSM-5 with different carbon content. (a) Total product yield and H₂O₂ conversion (X_{H2O2}(%)) and (b) total product yield normalized per H₂O₂ consumed. Reaction conditions: 30 mL of H₂O, 95 mL of CH₄ at 31 bar, 0.277 M H₂O₂, 100 mg of catalyst, reaction temperature = 30 °C, and reaction time = 1 h.

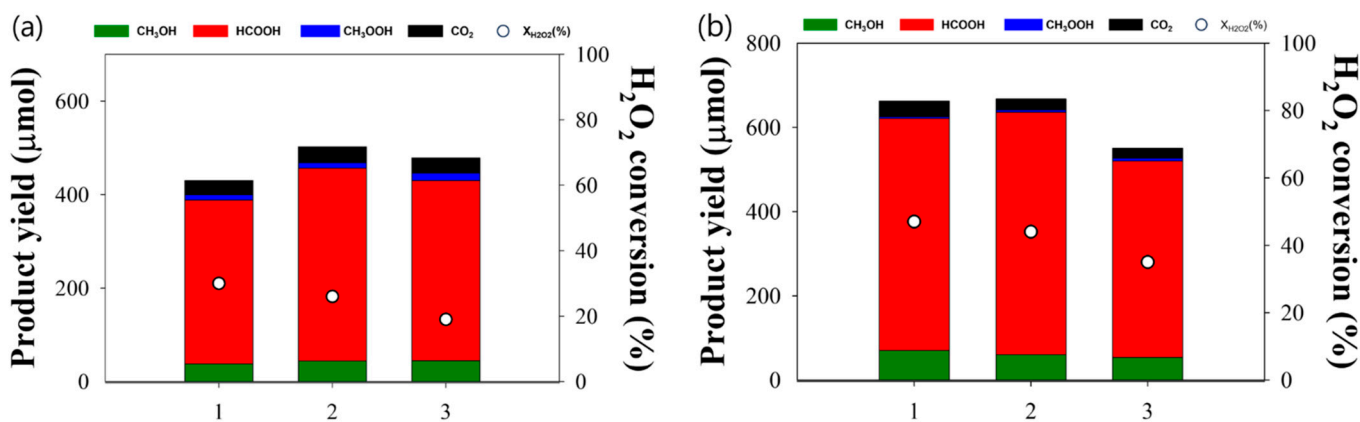


Figure 6. The recycling test with Fe-ZSM-5 (a) and C_{1.08}-Fe-ZSM-5 (b). Reaction conditions: 30 mL of H₂O, 95 mL of CH₄ at 31 bar, 0.277 M H₂O₂, 100 mg of catalyst, reaction temperature = 30 °C, and reaction time = 1 h.

From the characterization results, it was confirmed that the carbon coating primarily affected the textural properties (SSA_{BET}—micropore volume) and increased the surface hydrophobicity, while having a limited impact on the surface acidity of the catalyst. Noticeable enhancements in the product yield and H₂O₂ utilization efficiency were observed, particularly when the carbon content was more or less 0.50 wt.%. Previous reports have shown that the acidic sites on ZSM-5 can immobilize Fe species, with stronger acidity stabilizing more Fe species, thereby increasing the productivity of methane oxygenates [17]. However, in this study, we used the same parent Fe-ZSM-5 with a fixed amount of Fe species, and the surface acidity of Cx-Fe-ZSM-5 was comparable; therefore, the effect of surface acidity on productivity can be excluded.

The observed volcano relationships in Figures 4 and 5 can be mostly attributed to a combination of two factors: the positive effect of increased hydrophobicity and the negative effect of decreased textural properties. Hydrophobic surfaces facilitate the aggregation of hydrophobic substances, such as alkanes (e.g., methane), leading to a high local concentration of methane near the active sites [55–57]. Hydrophobic surfaces can also accelerate the adsorption of hydrophobic methane from the bulk phase to active sites within the pores.

These effects account for the improved product yields observed for the carbon-coated catalysts. However, the surface carbon coating can block the pores or poison the active sites, similar to the deactivation of coke. Pore blocking results in a decrease in textural properties, specifically SSA_{BET} . Indeed, the point at which the catalytic performance began to decrease coincided well with the point at which SSA_{BET} decreased (Figure S3, Figures 4 and 5). For instance, Cx-Fe-ZSM-5 exhibited similarly high catalytic performance within the 0.27–2.3 wt.% carbon content range. However, the catalytic performance declined abruptly when the carbon content exceeded this range. Similarly, the SSA_{BET} of Cx-Fe-ZSM-5 was comparable within the 0.27–2.3 wt.% carbon content range and then experienced a significant decrease beyond that. The trade-off between the positive hydrophobic effects and negative pore-blocking effects resulted in an optimal C0.62-Fe-ZSM-5 catalyst, which exhibited high catalytic performance with minimal carbon coating.

The current method of carbon coating offers several advantages over those previously reported. It does not require special equipment or reactive precursors, which are typically required for chemical vapor deposition [58] or hydrothermal carbonization [59]. Unlike the co-pyrolysis of biomass or polymers with ZSM-5 [60], FA is directly deposited on the external surface through simple and practical dry impregnation, allowing for an effective carbon coating with a small amount of FA. This enabled the fabrication of carbon-coated Fe-ZSM-5 catalysts with minimal pore blocking and significantly improved catalytic performance.

3. Experiment

3.1. Catalyst Preparation

$\text{NH}_4\text{-ZSM-5}$ (CBV 3024E) was purchased from Zeolyst (Kansas City, KS, USA). Iron (II) chloride tetrahydrate ($\text{FeCl}_2 \cdot 4\text{H}_2\text{O}$) and FA were obtained from Sigma Aldrich (Burlington, MA, USA) and used as received. The surface hydrophobicities of H-ZSM-5 and Fe-ZSM-5 were controlled by carbon coating, as shown in Scheme 1.

$\text{NH}_4\text{-ZSM-5}$ ($\text{SiO}_2/\text{Al}_2\text{O}_3 = 30$, Zeolyst) were calcined in air at 550 °C for 3 h to prepare H-ZSM-5. The prepared H-ZSM-5 was dried at 120 °C overnight in a vacuum oven. A specific amount of FA was deposited onto dried H-ZSM-5 using a dry impregnation method (Table S5). The FA-modified H-ZSM-5 was placed in an oven pre-set at 80 °C for 12 h. At this stage, the cross-linking reaction of FA occurs at the surface acid sites, resulting in the formation of poly(furfuryl alcohol) (PFA)-H-ZSM-5. Carbon-modified H-ZSM-5 was prepared by carbonizing PFA by heat treatment at 550 °C for 2 h in an argon atmosphere. The resulting catalysts are denoted as Cx-H-ZSM-5, where x represents the carbon content (wt.%). For example, C0.22-H-ZSM-5 implies carbon-coated H-ZSM-5 with a carbon content of 0.22 wt.%.

Briefly, 4.97 g of $\text{NH}_4\text{-ZSM-5}$ was added to 100 mL of an aqueous iron chloride solution containing 90.0 mg of $\text{FeCl}_2 \cdot 4\text{H}_2\text{O}$. This slurry was mixed at 60 °C for 3 h in a rotary evaporator. The water was removed through evaporation and then dried at 100 °C in an oven overnight and calcined in air at 550 °C for 3 h. To focus the discussion on the surface modification effect of Fe-ZSM-5, the Fe content was set to a constant value of 0.52%. The prepared 0.52 wt.% Fe-ZSM-5 was dried in a vacuum oven at 120 °C. A specific amount of FA was deposited onto dried Fe-ZSM-5 using a dry impregnation method (Table S5). The FA-modified Fe-ZSM-5 was placed in an oven pre-set at 80 °C for 12 h. At this stage, the cross-linking reaction of FA occurred at the surface acid sites, resulting in the formation of PFA-Fe-ZSM-5. Carbon-modified Fe-ZSM-5 was prepared by carbonizing PFA by heat treatment at 550 °C for 2 h in an argon atmosphere. The pyrolysis temperature was set to a constant temperature at 550 °C, and the same temperature was used for the preparation of Fe-ZSM-5. The resulting catalysts are denoted as Cx-Fe-ZSM-5, where x represents the carbon content (wt.%). For example, C0.27-Fe-ZSM-5 indicates carbon-coated Fe-ZSM-5 with a carbon content of 0.27 wt.%.

3.2. Catalytic Performance

Selective oxidation of methane in water was performed in an autoclave with a total volume of 125 mL. Water containing H₂O₂ (30 mL) and the catalyst (100 mg) were added to the reactor using a glass liner. The typical concentration of H₂O₂ was 0.277 M. After purging with methane five times at 31 bar, methane was charged at a pressure of 31 bar. The reaction was performed for 1 h with stirring at 1200 rpm. Two reaction temperatures were selected based on the type of catalyst used. The reaction was carried out at 50 °C for H-ZSM-5 and Cx-H-ZSM-5. In contrast, the reaction with Fe-ZSM-5 and Cx-Fe-ZSM-5 was performed at a relatively lower temperature of 30 °C due to their higher catalytic activity. This adjustment was necessary because, at 50 °C, there was complete H₂O₂ consumption (100% H₂O₂ conversion) with these catalysts. After the reaction, the temperature of the autoclave was rapidly cooled to 10 °C with liquid nitrogen. The stability of the two catalysts was investigated through recycling tests. After the reaction, the slurry was centrifuged to separate the liquid and solids. The solids were further used in the following reaction experiments. Methanol, methyl hydroperoxide, formic acid, and carbon dioxide are the main products. The gaseous product was separated using a PoraPLOT Q column (Agilent, Santa Clara, CA, USA), passed through a methanizer and quantified using a flame ionization detector in an online gas chromatograph (Younglin, Anyang, Korea). The liquid product was filtered through a microfilter (Millex, Darmstadt, Germany) and analyzed via ¹H-NMR (nuclear magnetic Resonance, Jeol (Tokyo, Japan) Resonance ECZ600R). Then, 0.1% trimethylsilylpropanoic acid (TMSP)/D₂O (Euriso-top, Saint-Aubin, France) was used as an external standard. The concentration of H₂O₂ in the liquid phase was analyzed at 210 nm using a liquid chromatograph (Younglin) equipped with a 100-5-C18 column (Kromasil, Bohus, Sweden) and an ultraviolet detector.

3.3. Characterization

The Fe content of the Fe-ZSM-5 catalyst was determined via inductively coupled plasma-optical emission spectroscopy using a Thermo Scientific (Waltham, MA, USA) iCAP 6500 instrument.

The carbon content of each catalyst was measured with TRSMCHNSC-6280TRSM (LECO, Joseph, MI, USA).

N₂ physisorption was performed using a Micromeritics ASAP 2020 (Hampton Bays, NY, USA) instrument to determine the Brunauer–Emmett–Teller (BET) specific surface area, micropore surface area, external surface area, pore volume, and micropore volume of the catalysts.

The surface acidity of the catalyst was probed by temperature-programmed desorption of ammonia (NH₃-TPD) using an AutoChem (Hampton Bays, NY, USA) 2910 unit (Micromeritics) equipped with a thermal conductivity detector and an online mass spectrometer (QMS 200, Pfeiffer Vacuum, Nashua, NH, USA). The mass-to-charge ratio of ammonia according to temperature was measured using mass spectrometry. A total of 0.10 g of sample was placed in a quartz U-tube, and each sample was pretreated in He at 600 °C for 1 h, then cooled to 150 °C, and held for 0.5 h. Adsorption was performed for 1 h with 3 vol.% NH₃/He flow, followed by physical desorption with He for 1 h. After cooling to 35 °C, the sample was heated to 600 °C at a heating rate of 10 °C/min and held at 600 °C for 1 h to perform NH₃-TPD with He.

The contact angles of the water droplets on the catalyst surface were measured using a high-speed camera (VEO-E 310 L, Phantom, San Francisco, CA, USA). The UV-Vis spectra of H-ZSM-5 and Fe-ZSM-5 were analyzed using a V-650 spectrophotometer (Jasco, Tokyo, Japan). Field emission-scanning electron microscopy (FE-SEM, FC-SM30, Hitachi, Tokyo, Japan) with energy-dispersive X-ray spectrometry was used to monitor the surface morphology of the carbon-coated catalysts and the distribution of each element.

The surface hydrophobicity of the catalyst was probed by temperature-programmed desorption of water (H₂O-TPD) using an AutoChem 2910 unit (Micromeritics) equipped with a thermal conductivity detector. A total of 10.0 mg of sample was placed in a quartz

U-tube, and each sample was pretreated in He at 500 °C for 1 h, then cooled to 30 °C, and held for 0.5 h. Adsorption of water was performed by the injection of 1 µL of deionized water in a He flow at 30 °C. After purging in a He flow for 1 h at 30 °C, the sample was heated to 500 °C at a heating rate of 10 °C/min and held at 500 °C for 1 h to perform H₂O-TPD with He.

The infrared studies were conducted with a Varian 670-IR (Varian, Inc., Beijing, China) using a transmission method. To enhance the signal-to-noise ratios, all samples were diluted with KBr using a KBr/sample ratio of 50:1 before loading into the cell. The system was equipped with a liquid nitrogen-cooled mercury–cadmium–telluride (MCT) detector. FTIR measurements were performed at a spectral resolution of 4 cm⁻¹, and spectra were truncated to retain the wavenumber range of 450 cm⁻¹ to 4000 cm⁻¹. Interferograms were processed using one level of zero filling, giving the spectra a data spacing of 2 cm⁻¹.

4. Conclusions

The surface hydrophobicities of H-ZSM-5 and Fe-ZSM-5 were controlled by varying the amount of FA using a straightforward carbon coating method. The outer surface of the parent material (e.g., H-ZSM-5 and Fe-ZSM-5) was impregnated, polycondensed, and carbonized, with FA having a molecular size larger than the micropore size of ZSM-5. With increasing carbon content, the textural properties (SSA_{BET} and pore volume) deteriorated, whereas the surface hydrophobicity increased. The catalytic performance for the aqueous-phase oxidation of methane with H₂O₂ increased with increasing carbon content, reaching a maximum value, and then decreased with a further increase in carbon content over carbon-coated H-ZSM-5 and Fe-ZSM-5. The total product yield normalized per H₂O₂ consumed also showed a trend similar to that of the carbon content, as did the catalytic performance. This implies that the surface hydrophobicity is an important factor affecting the catalytic activity for this reaction. Furthermore, the surface acidity of ZSM-5 decreased with the carbon content; therefore, the contribution of this surface passivation to the catalytic activity cannot be excluded, especially for carbon-coated Fe-ZSM-5 with low carbon contents.

Supplementary Materials: The following supporting information can be downloaded at: <https://www.mdpi.com/article/10.3390/catal14040280/s1>, Figure S1: UV-Vis spectra of H-ZSM-5 (a) and 0.52% Fe-ZSM-5 (b). The raw data and deconvoluted data are shown as a black line and a dashed line, respectively. Figure S2: SEM-EDX results of (a) C0.45-H-ZSM-5 and (b) C1.08-Fe-ZSM-5. Figure S3: The changes in surface area according to the carbon content in (a) Cx-H-ZSM-6 and (b) Cx-Fe-ZSM-5. Figure S4: The pore size distribution of (a) Cx-H-ZSM-5 and (b) Cx-Fe-ZSM-5. Figure S5: Deconvolution of NH₃-TPD profiles for H-ZSM-5 and carbon-coated H-ZSM-5 with different carbon contents. Figure S6: Deconvolution of NH₃-TPD profiles for Fe-ZSM-5 and carbon-coated Fe-ZSM-5 with different carbon contents. Figure S7: H₂O-TPD profiles for H-ZSM-5 and carbon-coated H-ZSM-5 with different carbon contents. Figure S8: FT-IR spectra for H-ZSM-5 and carbon-coated H-ZSM-5 (C2.70-H-ZSM-5). Figure S9: Product selectivity for partial oxidation of methane with H₂O₂ over H-ZSM-5 and Cx-H-ZSM-5. Figure S10: Product selectivity for partial oxidation of methane with H₂O₂ over H-ZSM-5 and Cx-Fe-ZSM-5. Table S1: The fraction of UV-Vis band for H-ZSM-5 and 0.52% Fe-ZSM-5. Table S2: The surface acid properties of H-ZSM-5 and carbon-coated H-ZSM-5 with different carbon contents. Table S3: The surface acid properties of Fe-ZSM-5 and carbon-coated Fe-ZSM-5 with different carbon contents. Table S4: The contact angle of the water droplet for H-ZSM-5, carbon-coated H-ZSM-5, Fe-ZSM-5, and carbon-coated Fe-ZSM-5. Table S5: The specific amount of furfuryl alcohol used for the synthesis of carbon-coated H-ZSM-5 and carbon-coated Fe-ZSM-5. Refs. [61,62] are cited in Supplementary Materials.

Author Contributions: Experimental investigation and data analysis, S.Y.H. and M.K.; writing—original draft preparation, S.Y.H.; supervision, writing—review and editing, J.H. and E.D.P.; project administration, and funding acquisition, E.D.P. All authors have read and agreed to the published version of the manuscript.

Funding: This work was supported by the C1 Gas Refinery Program through the National Research Foundation (NRF) of Korea funded by the Ministry of Science, ICT, and Future Planning (2015M3D3A1A01064899). This research was supported by H2KOREA, funded by the Ministry of Education (2022Hydrogen fuel cell-002, Innovative Human Resources Development Project for Hydrogen Fuel Cells).

Data Availability Statement: Data are contained within the article and Supplementary Materials.

Acknowledgments: We thank Eunyeong Yang (khy0881@ajou.ac.kr), Department of Chemical Engineering, Ajou University, for assistance with the H₂O-TPD experiment.

Conflicts of Interest: The authors declare no conflicts of interest.

References

1. Sung, D.M.; Kim, Y.H.; Park, E.D.; Yie, J.E. Role of Surface Hydrophilicity of Alumina in Methanol Dehydration. *Catal. Commun.* **2012**, *20*, 63–67. [[CrossRef](#)]
2. Vanoye, L.; Favre-Réguillon, A.; Munno, P.; Rodríguez, J.F.; Dupuy, S.; Pallier, S.; Pitault, I.; De Bellefon, C. Methanol Dehydration over Commercially Available Zeolites: Effect of Hydrophobicity. *Catal. Today* **2013**, *215*, 239–242. [[CrossRef](#)]
3. Li, D.; Wu, Z.; Zhou, D.; Xia, Y.; Lu, X.; He, H.; Xia, Q. One-Step Synthesis of Hybrid Zeolite with Exceptional Hydrophobicity to Accelerate the Interfacial Reaction at Low Temperature. *Microporous Mesoporous Mater.* **2019**, *280*, 195–202. [[CrossRef](#)]
4. Inagaki, S.; Takeyama, M.; Asanuma, K.; Yokose, Y.; Zhang, S.; Okuda, T.; Nakamura, K.; Nishi, Y.; Kubota, Y. Preparation of Hydrophobic Ti-Beta Catalyst Derived from Al-Rich Zeolite Beta Synthesized without Using Organic Structure-Directing Agent and Its Enhanced Catalytic Performance for Phenol Oxidation. *Microporous Mesoporous Mater.* **2022**, *346*, 112323. [[CrossRef](#)]
5. Wei, M.; Kuang, Y.; Duan, Z.; Li, H. The Crucial Role of Catalyst Wettability for Hydrogenation of Biomass and Carbon Dioxide over Heterogeneous Catalysts. *Cell Rep. Phys. Sci.* **2023**, *4*, 101340. [[CrossRef](#)]
6. Freakley, S.J.; Dimitratos, N.; Willock, D.J.; Taylor, S.H.; Kiely, C.J.; Hutchings, G.J. Methane Oxidation to Methanol in Water. *Acc. Chem. Res.* **2021**, *54*, 2614–2623. [[CrossRef](#)] [[PubMed](#)]
7. Dummer, N.F.; Willock, D.J.; He, Q.; Howard, M.J.; Lewis, R.J.; Qi, G.; Taylor, S.H.; Xu, J.; Bethell, D.; Kiely, C.J.; et al. Methane Oxidation to Methanol. *Chem. Rev.* **2023**, *123*, 6359–6411. [[CrossRef](#)] [[PubMed](#)]
8. Kang, J.; Park, E.D. Liquid-Phase Selective Oxidation of Methane to Methane Oxygenates. *Catalysts* **2024**, *14*, 167. [[CrossRef](#)]
9. Wang, V.C.C.; Maji, S.; Chen, P.P.Y.; Lee, H.K.; Yu, S.S.F.; Chan, S.I. Alkane Oxidation: Methane Monooxygenases, Related Enzymes, and Their Biomimetics. *Chem. Rev.* **2017**, *117*, 8574–8621. [[CrossRef](#)]
10. Hammond, C.; Jenkins, R.L.; Dimitratos, N.; Lopez-Sanchez, J.A.; Ab Rahim, M.H.; Forde, M.M.; Thetford, A.; Murphy, D.M.; Hagen, H.; Stangland, E.E.; et al. Catalytic and Mechanistic Insights of the Low-Temperature Selective Oxidation of Methane over Cu-Promoted Fe-ZSM-5. *Chem.—Eur. J.* **2012**, *18*, 15735–15745. [[CrossRef](#)]
11. Hammond, C.; Forde, M.M.; Ab Rahim, M.H.; Thetford, A.; He, Q.; Jenkins, R.L.; Dimitratos, N.; Lopez-Sanchez, J.A.; Dummer, N.F.; Murphy, D.M.; et al. Direct Catalytic Conversion of Methane to Methanol in an Aqueous Medium by Using Copper-Promoted Fe-ZSM-5. *Angew. Chem.—Int. Ed.* **2012**, *51*, 5129–5133. [[CrossRef](#)] [[PubMed](#)]
12. Hammond, C.; Dimitratos, N.; Lopez-Sanchez, J.A.; Jenkins, R.L.; Whiting, G.; Kondrat, S.A.; Ab Rahim, M.H.; Forde, M.M.; Thetford, A.; Hagen, H.; et al. Aqueous-Phase Methane Oxidation over Fe-MFI Zeolites; Promotion through Isomorphous Framework Substitution. *ACS Catal.* **2013**, *3*, 1835–1844. [[CrossRef](#)]
13. Hammond, C.; Dimitratos, N.; Jenkins, R.L.; Lopez-Sanchez, J.A.; Kondrat, S.A.; Hasbi Ab Rahim, M.; Forde, M.M.; Thetford, A.; Taylor, S.H.; Hagen, H.; et al. Elucidation and Evolution of the Active Component within Cu/Fe/ZSM-5 for Catalytic Methane Oxidation: From Synthesis to Catalysis. *ACS Catal.* **2013**, *3*, 689–699. [[CrossRef](#)]
14. Hutchings, G.J. Methane Activation by Selective Oxidation. *Top. Catal.* **2016**, *59*, 658–662. [[CrossRef](#)]
15. Peneau, V.; Armstrong, R.D.; Shaw, G.; Xu, J.; Jenkins, R.L.; Morgan, D.J.; Dimitratos, N.; Taylor, S.H.; Zanthoff, H.W.; Peitz, S.; et al. The Low-Temperature Oxidation of Propane by Using H₂O₂ and Fe/ZSM-5 Catalysts: Insights into the Active Site and Enhancement of Catalytic Turnover Frequencies. *ChemCatChem* **2017**, *9*, 642–650. [[CrossRef](#)]
16. Hammond, C.; Hermans, I.; Dimitratos, N. Biomimetic Oxidation with Fe-ZSM-5 and H₂O₂? Identification of an Active, Extra-Framework Binuclear Core and an FeIII-OOH Intermediate with Resonance-Enhanced Raman Spectroscopy. *ChemCatChem* **2015**, *7*, 434–440. [[CrossRef](#)]
17. Kalamaras, C.; Palomas, D.; Bos, R.; Horton, A.; Crimmin, M.; Hellgardt, K. Selective Oxidation of Methane to Methanol over Cu-And Fe-Exchanged Zeolites: The Effect of Si/Al Molar Ratio. *Catal. Lett.* **2016**, *146*, 483–492. [[CrossRef](#)]
18. Tomkins, P.; Ranocchiari, M.; Van Bokhoven, J.A. Direct Conversion of Methane to Methanol under Mild Conditions over Cu-Zeolites and Beyond. *Acc. Chem. Res.* **2017**, *50*, 418–425. [[CrossRef](#)] [[PubMed](#)]
19. Al-Shihri, S.; Richard, C.J.; Chadwick, D. Selective Oxidation of Methane to Methanol over ZSM-5 Catalysts in Aqueous Hydrogen Peroxide: Role of Formaldehyde. *ChemCatChem* **2017**, *9*, 1276–1283. [[CrossRef](#)]
20. Kim, M.S.; Park, K.H.; Cho, S.J.; Park, E.D. Partial Oxidation of Methane with Hydrogen Peroxide over Fe-ZSM-5 Catalyst. *Catal. Today* **2021**, *376*, 113–118. [[CrossRef](#)]

21. Kim, M.S.; Park, E.D. Aqueous-Phase Partial Oxidation of Methane with H_2O_2 over Fe-ZSM-5 Catalysts Prepared from Different Iron Precursors. *Microporous Mesoporous Mater.* **2021**, *324*, 111278. [[CrossRef](#)]
22. Zhu, K.; Liang, S.; Cui, X.; Huang, R.; Wan, N.; Hua, L.; Li, H.; Chen, H.; Zhao, Z.; Hou, G.; et al. Highly Efficient Conversion of Methane to Formic Acid under Mild Conditions at ZSM-5-Confining Fe-Sites. *Nano Energy* **2021**, *82*, 105718. [[CrossRef](#)]
23. Yu, T.; Li, Z.; Lin, L.; Chu, S.; Su, Y.; Song, W.; Wang, A.; Weckhuysen, B.M.; Luo, W. Highly Selective Oxidation of Methane into Methanol over Cu-Promoted Monomeric Fe/ZSM-5. *ACS Catal.* **2021**, *11*, 6684–6691. [[CrossRef](#)]
24. Lee, H.; Kwon, C.; Keum, C.; Kim, H.E.; Lee, H.; Han, B.; Lee, S.Y. Methane Partial Oxidation by Monomeric Cu Active Center Confined on ZIF-7. *Chem. Eng. J.* **2022**, *450*, 138472. [[CrossRef](#)]
25. Kim, M.S.; Yang, G.S.; Park, E.D. Effects of Cu Species on Liquid-Phase Partial Oxidation of Methane with H_2O_2 over Cu-Fe/ZSM-5 Catalysts. *Catalysts* **2022**, *12*, 1224. [[CrossRef](#)]
26. Lee, H.; Kwon, C.; Vikneshvaran, S.; Lee, S.; Lee, S.Y. Partial Oxidation of Methane to Methyl Oxygenates with Enhanced Selectivity Using a Single-Atom Copper Catalyst on Amorphous Carbon Support. *Appl. Surf. Sci.* **2023**, *639*, 158289. [[CrossRef](#)]
27. Lee, H.; Lee, S.Y. High Metal Loaded Cu(i)N₃ Single-Atom Catalysts: Superior Methane Conversion Activity and Selectivity under Mild Conditions. *J. Mater. Chem. A Mater.* **2023**, *11*, 15691–15701. [[CrossRef](#)]
28. Kang, J.; Park, E.D. Aqueous-Phase Selective Oxidation of Methane with Oxygen over Iron Salts and Pd/C in the Presence of Hydrogen. *ChemCatChem* **2019**, *11*, 4247–4251. [[CrossRef](#)]
29. Kang, J.; Puthiaraj, P.; Ahn, W.S.; Park, E.D. Direct Synthesis of Oxygenates via Partial Oxidation of Methane in the Presence of O₂ and H₂ over a Combination of Fe-ZSM-5 and Pd Supported on an Acid-Functionalized Porous Polymer. *Appl. Catal. A Gen.* **2020**, *602*, 117711. [[CrossRef](#)]
30. Kang, J.; Park, E.D. Selective Oxidation of Methane over Fe-Zeolites by In Situ Generated H₂O₂. *Catalysts* **2020**, *10*, 299. [[CrossRef](#)]
31. Wu, B.; Lin, T.; Huang, M.; Li, S.; Li, J.; Yu, X.; Yang, R.; Sun, F.; Jiang, Z.; Sun, Y.; et al. Tandem Catalysis for Selective Oxidation of Methane to Oxygenates Using Oxygen over PdCu/Zeolite. *Angew. Chem.—Int. Ed.* **2022**, *61*, e202204116. [[CrossRef](#)]
32. Yang, G.S.; Kang, J.; Park, E.D. Aqueous-Phase Partial Oxidation of Methane over Pd–Fe/ZSM-5 with O₂ in the Presence of H₂. *ChemCatChem* **2023**, *15*, e202201630. [[CrossRef](#)]
33. Kang, J.; Park, E.D. Partial Oxidation of Methane over Fe/ZSM-5 with Hydrogen Peroxide Generated in Situ over Pd/C in the Presence of Halide Ions. *Catal. Today* **2024**, *426*, 114367. [[CrossRef](#)]
34. Ab Rahim, M.H.; Forde, M.M.; Jenkins, R.L.; Hammond, C.; He, Q.; Dimitratos, N.; Lopez-Sanchez, J.A.; Carley, A.F.; Taylor, S.H.; Willock, D.J.; et al. Oxidation of Methane to Methanol with Hydrogen Peroxide Using Supported Gold-Palladium Alloy Nanoparticles. *Angew. Chem.—Int. Ed.* **2013**, *52*, 1280–1284. [[CrossRef](#)] [[PubMed](#)]
35. Ab Rahim, M.H.; Armstrong, R.D.; Hammond, C.; Dimitratos, N.; Freakley, S.J.; Forde, M.M.; Morgan, D.J.; Lalev, G.; Jenkins, R.L.; Lopez-Sanchez, J.A.; et al. Low Temperature Selective Oxidation of Methane to Methanol Using Titania Supported Gold Palladium Copper Catalysts. *Catal. Sci. Technol.* **2016**, *6*, 3410–3418. [[CrossRef](#)]
36. He, Y.; Luan, C.; Fang, Y.; Feng, X.; Peng, X.; Yang, G.; Tsubaki, N. Low-Temperature Direct Conversion of Methane to Methanol over Carbon Materials Supported Pd-Au Nanoparticles. *Catal. Today* **2020**, *339*, 48–53. [[CrossRef](#)]
37. He, Y.; Liang, J.; Imai, Y.; Ueda, K.; Li, H.; Guo, X.; Yang, G.; Yoneyama, Y.; Tsubaki, N. Highly Selective Synthesis of Methanol from Methane over Carbon Materials Supported Pd-Au Nanoparticles under Mild Conditions. *Catal. Today* **2020**, *352*, 104–110. [[CrossRef](#)]
38. Yan, Y.; Chen, C.; Zou, S.; Liu, J.; Xiao, L.; Fan, J. High H₂O₂ Utilization Promotes Selective Oxidation of Methane to Methanol at Low Temperature. *Front. Chem.* **2020**, *8*, 252. [[CrossRef](#)] [[PubMed](#)]
39. Wu, B.; Huang, M.; Yu, X.; Liu, J.; Lin, T.; Zhong, L. Selective Oxidation of Methane to Oxygenates Using Oxygen via Tandem Catalysis. *Chem.—Eur. J.* **2023**, *29*, e202203057. [[CrossRef](#)]
40. Ni, F.; Richards, T.; Smith, L.R.; Morgan, D.J.; Davies, T.E.; Lewis, R.J.; Hutchings, G.J. Selective Oxidation of Methane to Methanol via In Situ H₂O₂ Synthesis. *ACS Org. Inorg. Au* **2023**, *3*, 177–183. [[CrossRef](#)]
41. Jin, Z.; Wang, L.; Zuidema, E.; Mondal, K.; Zhang, M.; Zhang, J.; Wang, C.; Meng, X.; Yang, H.; Mesters, C.; et al. Hydrophobic Zeolite Modification for in Situ Peroxide Formation in Methane Oxidation to Methanol. *Science* **2020**, *367*, 193–197. [[CrossRef](#)] [[PubMed](#)]
42. Centi, G.; Perathoner, S.; Pino, F.; Arrigo, R.; Giordano, G.; Katovic, A.; Pedulà, V. Performances of Fe-[Al, B]MFI Catalysts in Benzene Hydroxylation with N₂O: The Role of Zeolite Defects as Host Sites for Highly Active Iron Species. *Catal. Today* **2005**, *110*, 211–220. [[CrossRef](#)]
43. Forde, M.M.; Armstrong, R.D.; McVicker, R.; Wells, P.P.; Dimitratos, N.; He, Q.; Lu, L.; Jenkins, R.L.; Hammond, C.; Lopez-Sanchez, J.A.; et al. Light Alkane Oxidation Using Catalysts Prepared by Chemical Vapour Impregnation: Tuning Alcohol Selectivity through Catalyst Pre-Treatment. *Chem. Sci.* **2014**, *5*, 3603–3616. [[CrossRef](#)]
44. Joo, S.; Choi, S.; Oh, I.; Kwak, J.; Liu, Z.; Terasaki, O.; Ryoo, R. Ordered nanoporous arrays of carbon supporting high dispersions of platinum nanoparticles. *Nature* **2001**, *412*, 169–172. [[CrossRef](#)] [[PubMed](#)]
45. Al-Dughaither, A.S.; De Lasas, H. HZSM-5 Zeolites with Different SiO₂/Al₂O₃ Ratios. Characterization and NH₃ Desorption Kinetics. *Ind. Eng. Chem. Res.* **2014**, *53*, 15303–15316. [[CrossRef](#)]
46. Song, Y.; Zhu, X.; Xie, S.; Wang, Q.; Xu, L. The Effect of Acidity on Olefin Aromatization over Potassium Modified ZSM-5 Catalysts. *Catal. Lett.* **2004**, *97*, 31–36. [[CrossRef](#)]

47. Han, Y.; Lu, C.; Xu, D.; Zhang, Y.; Hu, Y.; Huang, H. Molybdenum Oxide Modified HZSM-5 Catalyst: Surface Acidity and Catalytic Performance for the Dehydration of Aqueous Ethanol. *Appl. Catal. A Gen.* **2011**, *396*, 8–13. [[CrossRef](#)]
48. Putluru, S.S.R.; Schill, L.; Jensen, A.D.; Fehrmann, R.S.N. Selective Catalytic Reduction of NO_x with NH₃ on Cu-, Fe-, and Mn-Zeolites Prepared by Impregnation: Comparison of Activity and Hydrothermal Stability. *J. Chem.* **2018**, *2018*, 8614747. [[CrossRef](#)]
49. Bagnasco, G. Improving the Selectivity of NH₃ TPD Measurements. *J. Catal.* **1996**, *159*, 249–252. [[CrossRef](#)]
50. Katada, N.; Niwa, M. Analysis of Acidic Properties of Zeolitic and Non-Zeolitic Solid Acid Catalysts Using Temperature-Programmed Desorption of Ammonia. *Catal. Surv. Asia* **2004**, *8*, 161–170. [[CrossRef](#)]
51. Xu, S.; Sheng, H.; Ye, T.; Hu, D.; Liao, S. Hydrophobic Aluminosilicate Zeolites as Highly Efficient Catalysts for the Dehydration of Alcohols. *Catal. Commun.* **2016**, *78*, 75–79. [[CrossRef](#)]
52. Han, X.; Wang, L.; Li, J.; Zhan, X.; Chen, J.; Yang, J. Tuning the Hydrophobicity of ZSM-5 Zeolites by Surface Silanization Using Alkyltrichlorosilane. *Appl. Surf. Sci.* **2011**, *257*, 9525–9531. [[CrossRef](#)]
53. Catuzo, G.L.; Santilli, C.V.; Martins, L. Hydrophobic-Hydrophilic Balance of ZSM-5 Zeolites on the Two-Phase Ketalization of Glycerol with Acetone. *Catal. Today* **2021**, *381*, 215–223. [[CrossRef](#)]
54. Cavuoto, D.; Zaccheria, F.; Ravasio, N. Some Critical Insights into the Synthesis and Applications of Hydrophobic Solid Catalysts. *Catalysts* **2020**, *10*, 1337. [[CrossRef](#)]
55. Wang, H.; Xin, W.; Wang, Q.; Zheng, X.; Lu, Z.; Pei, R.; He, P.; Dong, X. Direct Methane Conversion with Oxygen and CO over Hydrophobic DB-ZSM-5 Supported Rh Single-Atom Catalyst. *Catal. Commun.* **2022**, *162*, 106374. [[CrossRef](#)]
56. Zhang, Q.; Yu, J.; Corma, A. Applications of Zeolites to C1 Chemistry: Recent Advances, Challenges, and Opportunities. *Adv. Mater.* **2020**, *32*, e2002927. [[CrossRef](#)] [[PubMed](#)]
57. Zapata, P.A.; Faria, J.; Ruiz, M.P.; Jentoft, R.E.; Resasco, D.E. Hydrophobic Zeolites for Biofuel Upgrading Reactions at the Liquid-Liquid Interface in Water/Oil Emulsions. *J. Am. Chem. Soc.* **2012**, *134*, 8570–8578. [[CrossRef](#)] [[PubMed](#)]
58. Kim, K.; Lee, T.; Kwon, Y.; Seo, Y.; Song, J.; Park, J.K.; Lee, H.; Park, J.Y.; Ihee, H.; Cho, S.J.; et al. Lanthanum-Catalysed Synthesis of Microporous 3D Graphene-like Carbons in a Zeolite Template. *Nature* **2016**, *535*, 131–135. [[CrossRef](#)]
59. Wang, Y.; Guerra, P.; Zaker, A.; Maag, A.R.; Tompsett, G.A.; Smith, L.J.; Huang, X.; Bond, J.Q.; Timko, M.T. Strategies for Extending Zeolite Stability in Supercritical Water Using Thermally Stable Coatings. *ACS Catal.* **2020**, *10*, 6623–6634. [[CrossRef](#)]
60. Zhao, T.; Wei, Y.; Wang, J.; Wang, Q.; Chen, Y.; Liu, X.; Zhao, Y. Microporous Carbon Coated Zeolite Particles for Efficient Carbon Capture from Wet Flue Gas. *Sep. Purif. Technol.* **2023**, *317*, 123762. [[CrossRef](#)]
61. Asghari, A.; Khorrami, M.K.; Kazemi, S.H. Hierarchical H-ZSM5 zeolites based on natural kaolinite as a high-performance catalyst for methanol to aromatic hydrocarbons conversion. *Sci. Rep.* **2019**, *9*, 17526. [[CrossRef](#)] [[PubMed](#)]
62. Setyaningrum, D.L.; Riyanto, S.; Rohman, A. Analysis of corn and soybean oils in red fruit oil using FTIR spectroscopy in combination with partial least square. *Int. Food Res. J.* **2013**, *20*, 1977–1981.

Disclaimer/Publisher’s Note: The statements, opinions and data contained in all publications are solely those of the individual author(s) and contributor(s) and not of MDPI and/or the editor(s). MDPI and/or the editor(s) disclaim responsibility for any injury to people or property resulting from any ideas, methods, instructions or products referred to in the content.